Sensing of Volatile Organic Compounds on Two-Dimensional Nitrogenated Holey Graphene, Graphdiyne, and Their Heterostructure

Tanveer Hussain[*1], Muhammad Sajjad[2], Deobrat Singh[3], Hyeonhu Bae[4]
Hoonkyung Lee[4], J. Andreas Larsson[2], Rajeev Ahuja,[3,5] and Amir Karton[1]

[1]School of Molecular Sciences, The University of Western Australia, Perth, WA 6009, Australia
[2]Applied Physics, Division of Materials Science, Department of Engineering Sciences and Mathematics, Luleå University of Technology, SE-97187 Luleå, Sweden
[3]Condensed Matter Theory Group, Department of Physics and Astronomy,
Box 516, Uppsala University, S-75120 Uppsala, Sweden
[4]Department of Physics, Konkuk University, Seoul 05029, Republic of Korea
[5]Applied Materials Physics, Department of Materials and Engineering,
Royal Institute of Technology (KTH), S-100 44 Stockholm, Sweden

Abstract

Gas-sensing properties of nitrogenated holey graphene (C_2N), graphdiyne (GDY) and their van der Waals heterostructure (C_2N···GDY) have been studied towards particular volatile organic compounds (VOCs) by means of spin-polarized, dispersion-corrected DFT calculations. We find that VOCs such as acetone, ethanol, propanal, and toluene interact weakly with the GDY monolayer; however, the bindings are significantly enhanced with the C_2N monolayer and the hybrid C_2N···GDY heterostructure in AB stacking. Electron localization function (ELF) analysis shows that all VOCs are van der Waals bound (physical binding) to the 2D materials, which result in significant changes of the charge density of C_2N and GDY monolayers and the C_2N···GDY heterostructure. These changes alter the electronic properties of C_2N and GDY, and the C_2N···GDY heterostructure, upon VOC adsorption, which are investigated by density of states plots. We further apply thermodynamic analysis to study the sensing characteristics of VOCs under varied conditions of pressure and temperature. Our findings clearly indicate that the C_2N···GDY heterostructure is a promising material for sensing of certain VOCs.

Key words: 2D monolayers, 2D Heterostructures, Gas-sensing, DFT.

Cite as:
T. Hussain, M. Sajjad, D. Singh, H. Bae, H. Lee, J. A. Larsson, R. Ahuja, A. Karton, *Carbon*, 163, 213–223 (2020). https://doi.org/10.1016/j.carbon.2020.02.078

Introduction

Efficient detection and capture of environmental pollutants, like volatile organic compounds (VOCs), is important due their considerable abundance in indoor environments and negative effects on human health.**[1, 2]** For example, exposure to certain VOCs has been found to be correlated with various cancers, which makes them an important target for detection and capturing.**[3]** Among various VOCs, detection of acetone, ethanol, propanol, and toluene is of particular interest due to their relevance in areas such as diabetes diagnostics, breath tests, toxicity, and environmental protection.**[4, 5]** In addition, the selected molecules model a wide range of prototypical aldehydes, keto, alcohol, and aromatic functionalities commonly found in VOCs.

Various nano-materials have been considered for VOC sensing, for example metal-oxide-based gas sensors, which have significant advantages over conventional techniques such as mass spectrometry and gas chromatography. **[6]** Metal oxides such as TiO_2, ZnO, In_2O_3 and many others have been used in this regard. However, their limited resolution and sensitivity in the range of parts per million (ppm) limits the applicability of this class of gas sensors.

The promise of two-dimensional (2D) materials, especially graphene, spans across many fields due to their attractive properties such as large surface area, robust carrier mobilization and charge transport, thermal stabilities and mechanical strength. **[7-11]** These chemical and physical properties make graphene an attractive material for a range of applications including gas sensing. **[12-15]** However, the zero-band gap limits the application of graphene (in its pristine form) in nanoelectronics. This limitation motivated the design and synthesis of various graphene-like 2D materials having intrinsic energy band gaps. Graphdiyne (GDY) and nitrogenated holey graphene (C_2N) monolayers are two such materials that possess fascinating structural and electronic properties and have found significant interest in scientific and technological fields due to their porous structures. **[16-18]**

GDY, an sp/sp^2 co-hybridized monolayer of carbon atoms with large triangular pores, **[19]** is a promising material in various applications due to its structural, electronic, and mechanical properties. **[20-23]** Prominent applications include gas separation and capture **[24]** and selective extraction of H_2, He, and O_2. **[25-28]** In addition to gas-membrane applications, GDY has been found to have

potential use as an efficient water purification material. **[29]** C_2N is a 2D material composed of phenyl and pyrazine rings. Similar to GDY, the C_2N monolayer has large uniformly distributed pores. The presence of intrinsic band gap and the existence of N-containing pores make C_2N useful in many applications including gas sensing. **[30-33]**

In the context of gas-phase chemistry, so far the applications of both GDY and C_2N monolayers have been restricted to either membranes for the separation of gases or capture small molecules like CO_2, HF, HCl and H_2S. To the best of our knowledge, the gas-sensing properties of a hybrid C_2N···GDY material towards VOCs have not been reported. To bridge this gap, we investigate here the structural, electronic, and VOC sensing properties of GDY, C_2N and C_2N···GDY heterostructures by means of density functional theory (DFT) calculations. Our van der Waals corrected DFT calculations indicate that VOCs bind to C_2N and C_2N···GDY heterostructures with relatively high binding energies and results in detectable changes in the electronic properties.

Computational details

Spin-polarization DFT calculations were performed using the Vienna *Ab initio* Simulation Package (VASP). **[34, 35]** The generalized gradient approximation (GGA) PBE exchange-correlation functional was used in conjunction with the projector-augmented wave (PAW) method to account for electron-ion interactions. **[36, 37]** Since GGA methods involve short-range correlation they tend to significantly underestimate dispersion interactions unless dispersion corrections are added. Here we used the empirical DFT-D3 dispersion correction of Grimme *et al.* **[38]** A cut-off energy of 500 eV was used for the plane wave basis set. We used 2□2 supercells of both GDY and C_2N monolayers having 72 atoms each with a vacuum of 20 Å along the perpendicular directions to avoid unwanted interactions along the vertical z-direction. We used the Monkhorst-Pack scheme for the sampling the Brillouin zone with a mesh size of 5□5□1 for geometry optimizations and a thicker mesh of 9□9□1 for the density of states (DOS) calculations. **[39]** The systems were optimized until a convergence criterion of 10^{-6} eV was reached and forces were less than 0.01 eV/Å.

Results and discussion

First, we will briefly describe the structural properties of the optimized C_2N and GDY monolayers. The lattice constant of C_2N is found to be 8.33 Å. There are two types of rings in the C_2N monolayer namely, benzene rings and pyrazine rings, with C–C bond lengths of 1.34 and 1.43 Å, respectively, whereas the C–N bond length is 1.47 Å, all of these values agree well with previous studies using same level of DFT calculations. **[30, 40]** In the case of GDY, we found the lattice constant, C–C (small pore) and C–C (big-pore) bond lengths to be 9.46, 1.43 and 1.39 Å, respectively, in good agreement with previous studies. **[20, 21]** In their ground state configurations the pore diameters of C_2N and GDY are found to be 5.52 and 8.02 Å, respectively. **[20, 40]** The optimized structures of the C_2N and GDY monolayers are shown in Figures 1(a) and 2(a), respectively. Top and side view of the C_2N···GDY heterostructure in the most favorable (AB) stacking is shown in Figure 3(a).

The selected VOCs (acetone, ethanol, propanol and toluene) can bind on C_2N, GDY, and C_2N···GDY surfaces at multiple binding sites and in several orientations. We therefore considered all the available binding sites and all possible orientations in each case in order to identify the energetically most stable configurations. The binding energies (E_b) are calculated using the following relation

$$E_b = E(VOC@2D) - E(2D) - E(VOC);\ 2D = C_2N,\ GDY,\ C_2N\ldots GDY \qquad (1)$$

In equation 1, the first, second and third terms represent the total energies of VOC@2D (2D = C_2N, GDY, C_2N…GDY), 2D and VOC, respectively. The binding energies and binding distances of the VOCs are given in Table 1. In the following discussion we describe the binding characteristics of the VOCs in each system.

Figure 1(b-e) shows top and side views of the energetically most favorable orientations of the VOCs bound onto pristine C_2N monolayer. In the most favorable configuration, acetone binds with C_2N in such a way that one of C–H bonds is pointing towards the big pore of C_2N with an E_b value of -0.50 eV and a binding distance of 2.69 Å between the hydrogen and the sheet. In contrast, ethanol binds to the sheet in a vertical orientation with the hydroxyl hydrogen pointing towards the big pore of C_2N at a distance Δd of 2.53 Å and an E_b value of -0.52 eV (Figure 1c). Furthermore, unlike acetone which is placed closer to the edge of the big pore with

the oxygen atom pointing outward (Figure 1b), the ethanol oxygen is positioned above the center of the pore. Similar to acetone, propanal lies above the pore with the oxygen atom pointing outward (Figure 1d). In this case, the carbonyl hydrogen is pointing towards the big pore. The E_b and Δd are -0.52 eV and 2.42 Å, respectively, which shows that the binding of ethanol and propanol with C_2N is the strongest among the studied VOCs. Toluene binds with C_2N vertically such that the para H atom points towards the sheets exactly above the center of the big pore with E_b and Δd values of -0.40 eV and 2.99 Å, respectively, which is the weakest binding coupled with the largest distance among all the VOCs studied.

We have used electron localization function (ELF) analysis to study the binding interactions between the VOCs and 2D surfaces. In all cases this binding involves van der Waals (vdW), polarization, and dispersion interactions. This is characterized in ELF by the contraction of the electron densities at the interaction interface. To further understand the binding we have employed Bader charge analysis to investigate the amount of charge transfer between the VOCs and C_2N. This analysis indicates negligibly amounts of charge transfer between the VOCs and C_2N (namely, of 0.01, 0.02, 0.01 and 0.03 *e* for acetone, ethanol, propanal and toluene, respectively). We thus conclude that charge transfer does not significantly contribute to the binding. However, a careful charge analysis reveals charge rearrangements within the C_2N sheet upon VOC binding. For example, in the case of acetone binding to the C_2N sheet, the C and N atoms of C_2N closet to the acetone oxygen loose charges 0.07 and 0.10 *e,* respectively, which are transferred to the neighboring C atoms. Depletion and accumulation of charge due to these effects can be seen in the isosurface charge difference densities (CDD) in Figure 4(a-d). A further analysis of these changes in the electronic structures is reported below in a separate section under the heading electronic properties.

The VOCs@GDY interactions result in weaker binding (smaller E_b values) compared to C_2N, which could be due to the lack of polar bonds in GDY. Similar to the acetone@C_2N, acetone binds to GDY with the methyl group pointing towards the center of the big pore with E_b and Δd values of -0.25 eV and 2.88 Å, respectively. The most favorable configuration of ethanol@GDY is similar to that of ethanol@C_2N, with the OH hydrogen atom above the center of the big pore and pointing towards the GDY. However, the E_b value is reduced significantly to -0.23 eV at a Δd of 2.76 Å.

Propanal interacts with GDY in a tilted manner, similarly to the proponal@C_2N binding, but with a significantly smaller E_b value of -0.28 eV and longer Δd value of 3.13 Å. Finally, the toluene@GDY interaction takes place with the toluene molecule lying flat (horizontal) above the center of the big pore, which was not the most stable configuration for toluene@C_2N where the molecule binds vertically. Nevertheless, the resultant E_b value of -0.34 eV is comparable to toluene@C_2N binding of -0.40 eV. The shortest Δd for toluene is found to be 3.01 Å. It is evident from the above binding energies that, with the exception of toluene, the binding strength of VOCs on GDY is less than half of that on C_2N. For toluene, on the other hand, the binding strength with GDY is only slightly smaller than that with C_2N.

Figure 2(b-e) shows top and side views of the optimized structures of GDY bound with the selected VOCs. Bader charge analysis shows no significant charge transfer between the VOCs and GDY sheet (namely, for all VOCs 0.02 *e* have been transferred to GDY). Isosurface CDD as shown in Figure 5 (a-d) demonstrate the depletion and accumulation of these charge density due to the physical binding.

After studying the binding of the selected VOCs on the monolayers of C_2N and GDY, we turn to the binding of VOCs on to the C_2N···GDY heterostructure. For this purpose, we constructed several C_2N···GDY heterostructures by considering different stacking and interlayer spacing. The lowest energy configuration of C_2N···GDY is shown is in Figure 3 (a) with C_2N as the bottom and GDY as the top layer with an interlayer spacing of 3.54 Å in AB stacking. In order to find out the most stable binding configurations, the VOCs were introduced to all the available binding sites on the C_2N···GDY heterostructure, in the same way as was done for the C_2N and GDY monolayers.

The optimized structures of the VOCs on C_2N···GDY heterostructure are shown in Figure 3 (b-e). Acetone binds with C_2N···GDY with the methyl group placed at the edge of the big pore, which is different to that of both C_2N and GDY monolayers, where it is placed at the center of the big pore. The E_b value for the most preferential configurations is -0.51 eV at a Δd of 3.01 Å, which is significantly stronger than acetone binding on a GDY monolayer. Ethanol also binds with the CH_3 group above the corner of the big pore of GDY, with E_b and Δd values of -0.49 eV and 3.02 Å, respectively. The orientation of the adsorbed ethanol molecule is similar to that of acetone rather than binding through the OH hydrogen as in the case of C_2N

and GDY monolayers. In the lowest energy configurations, propanal sits above the side of the big pore of the C_2N···GDY heterostructure like acetone, however it prefers to be close to the small hexagonal ring having E_b and Δd values of -0.57 eV and 2.96 Å, respectively. Finally, toluene is placed horizontally above the hexagonal ring of GDY with E_b and Δd values of -0.77 eV and 2.86 Å, respectively. Thus, the E_b value for toluene is the strongest among all the molecules on all the systems considered in this study. In summary, the results above demonstrate that inserting a C_2N monolayer underneath GDY significantly increases the bonding energy with VOCs relative to a single GDY monolayer. The largest increase in binding energy is observed for toluene.

In addition, it is of interest to calculate the binding energies of the VOCs on the C_2N layer in the C_2N···GDY heterostructure. The binding energies (E_b) of acetone, ethanol, propanal and toluene are found to be -0.15, -0.24, -0.16, and -0.35 eV, respectively. These binding energies are considerably smaller than those of the VOCs bound on the GDY side, which are E_b = -0.51, -0.49, -0.57, and -0.77 eV for acetone, ethanol, propanal and toluene, respectively. We therefore conclude that the GDY side is more suitable for gas-sensing purposes.

Finally, it is of interest to compare the calculated E_b values of VOCs on the C_2N···GDY heterostructure, which exhibits the strongest VOC binding among the considered systems, with the previous experimental and theoretical results. For example, the E_b value of -0.51 eV obtained here for acetone on the C_2N···GDY heterostructure is significantly stronger than E_b values obtained at the same level of theory used here for acetone on other 2D materials: -0.37 (graphene), -0.33 (black phosphorene), -0.22 (MoS_2), -0.32 ($Ti_3C_2O_2$) and -0.31 eV ($Ti_3C_2F_2$). **[41]** On the other hand, in the same study they obtained an E_b value for acetone on $Ti_3C_2(OH)_2$ of -0.77 eV, which is still in the desired energetic range for gas-sensing.

We find that ethanol binds with the C_2N···GDY heterostructure with an E_b of -0.49 eV which is twice as strong as its binding on black phosphorene with an E_b value of -0.24 eV obtained at the same the level of theory used in the present study. **[42]** We also note that in contrast to our C_2N···GDY heterostructure which binds ethanol effectively in its pristine form, it has been experimentally shown that pristine and Fe-doped ZnO surfaces cannot detect the presence of ethanol at room temperature. **[43]**

A recent experimental study by Zhang et al. revealed that pristine form of pecan-kernel like TiO_2 material could not respond to toluene. **[44]** This could be due to insufficient binding of toluene with TiO_2 in its pure form. In contrast, the C_2N···GDY heterostructure binds toluene with an E_b value of -0.77 eV.

Given the promising results obtained for the C_2N···GDY heterostructure, it is important to also consider the bilayers of C_2N and GDY in order to confirm that the optimal VOC binding is not a multilayer effect. For this purpose we have considered the case of acetone binding on the bilayers of C_2N and GDY. The E_b value of acetone on C_2N and GDY bilayers are found to be -0.11 and -0.28 eV, respectively. These E_b values are considerably smaller than acetone binding on C_2N···GDY heterostructure with E_b value of -0.51 eV. This clearly indicates that the VOCs binding on C_2N···GDY heterostructure is more promising than that of C_2N and GDY bilayers.

Figure 11 show the ELF analysis, which reveals the binding mechanism to be physical binding and Bader charge analysis shows small amounts of charge transfer (namely, 0.03, 0.03, 0.03 and 0.05 *e* have been transferred to C_2N···GDY heterostructure from acetone, ethanol, propanal and toluene, respectively). It is noted that these values are slightly higher than those for the VOCs on C_2N and GDY monolayers. Figure 6(a-d) shows the depletion and accumulation of charges due to the physical binding plotted through isosurface CDD of acetone, ethanol, propanal and toluene, on the C_2N···GDY heterostructure.

Before turning to the effect of VOC binding on the electronic properties of the C_2N and GDY monolayers and their hetrostructure a comment is due on the possibility of VOC binding to vacancy defects. We consider here both C and N vacancies. As expected VOCs bind very strongly to these vacancy defect sites forming covalent bonds with the surface. These strong binding energies will render such defect sites from being able to reversibly detect VOCs, however, once a VOC binds to these sites they will be passivized and would not influence the sensing behavior of the pristine parts of the 2D material.

Electronic properties

Here we turn to the influence of VOCs adsorption on the electronic properties of the 2D materials. We note that in this analysis the geometries of VOC@2D, bare 2D monolayers and VOCs are fully optimized. To understand the character of

electrons involved in the valence band maximum (VBM) and conduction band minimum (CBM) and also the origin of band gap narrowing for the VOCs (acetone, ethanol, propanol and toluene) due to the absorption on the C_2N monolayers, the total (TDOS) and projected density of states (PDOS) were computed and depicted in Figure 7. The calculated PDOS given in Figure 7(a) shows that the VBM of the pristine C_2N monolayer mainly originates from the hybridization of C(2p) and N(2p) states, whereas the CBM is dominated by N(2p) states with a noticeable contribution from C(2p) states. Figure 7(a) shows a band gap of 1.66 eV for pristine C_2N, in agreement with previous PBE results of the band gap value in the C_2N monolayer **[45]**. We find that the TDOS (see Figure 7(b) and (d)) for either the valence or conduction band of C_2N monolayer is not significantly influenced upon acetone and propanol molecule adsorption, which is consistent with their van der Waals binding. The energy states from acetone and propanol are located at the deep energy level around 3 eV below the Fermi level (valence band) and 4 eV above the Fermi level (conduction band), as shown in Figure 7(b) and (d). However, we can still see the state differences for the organic molecules on the surface of C_2N monolayer, both the CBM and VBM edges are relatively shifted downward (see Figure 7(b-e) due to the presence of the physisorbed VOCs. In the case of ethanol and toluene adsorption on C_2N, as depicted in Figure 7(c-e), there is noticeable upward shift of the valence band edges while the conduction band edges shift toward higher energy values and appear around 5 eV. Moreover, the electronic structure computed for a GDY sheet is shown in Figure 8(a). The band dispersion appears mostly from the overlap of the carbon 2p orbitals. It is seen that the graphdiyne monolayer is a semiconductor with a band gap of 0.46 eV, which is consistent with the previous work **[46]**. The revealed electronic difference and distinct adsorption behavior on GDY imply the possibilities to design new and superior gas sensors based on GDY. Some electronic states appear near the Fermi level around -1 eV to 0 eV in valence band for each case (acetone, ethanol, propanol and toluene) as shown in Fig. 8 (b-e). These peaks are due to the hybridization of the LUMO levels of the organic molecules with the states of GDY. The conduction band also influenced by organic molecule absorption on graphdiyne surface and states seems above the 3 eV.

Here we analyze the electronic properties of the C_2N···GDY vdW heterostructure. As a reference, the PDOS of C_2N and GDY monolayers are also

computed and presented in Figures 7(a) and 8(a), respectively. PDOS show that the both the monolayers are direct band gap semiconductors, and the band gaps are 1.66 and 0.46 eV for C_2N and GDY, respectively. The projected DOS of the C_2N···GDY heterostructure is given in Figure 9(a) in which the black C1 (p) color indicate GDY layer, red and green C2 (p) and N (p) color indicate the contributions from the C_2N layer. As one can see, the C_2N···GDY heterostructure is a semiconductor with a band gap of 0.43 eV. Its VBM and CBM mainly originate from 2p states of GDY, indicating that a type-II heterostructure is formed. To further investigate the adsorption mechanisms of acetone, ethanol, propanol and toluene organic molecules adsorbed on the C_2N···GDY heterostructure, we plot the total density of states (DOS) and projected density of states (PDOS) in Figure 9(b-e). Noticeably, the main electronic level contributions of acetone to the total system localize around ◘3 eV in the valence band, 3.5 eV in the conduction band, which is away from the Fermi level. The electrons are slightly shared between C_2N···GDY heterostructure and acetone, which shows the intensity of the interaction between the acetone molecule and the C_2N···GDY heterostructure. The contribution of the ethanol, propanol and toluene electronic levels to the DOS of whole systems is localized around 4 eV in the conduction bands that away from the Fermi level and −1 eV in the valence bands where is very near away to the Fermi level. Finally, we found that the broadening peak around -4 eV in the valence band is due to the hybridization of states away from the Fermi level of organic molecules with the states of C_2N···GDY. Due to the presence of electronic states near the Fermi level with the influence of organic molecules, C_2N···GDY heterostructure are better candidates for sensing nanodevices.

Thermodynamic analysis

Determination of gas capacity under the practical conditions of pressure and temperature and under various compositions is important for the evaluation of sensor/adsorbent. Thermodynamic analysis of each of the VOCs (acetone, ethanol, propanal, toluene) on C_2N, GDY and C_2N···GDY heterostructure was carried out to estimate their practical sensing abilities at a given temperature and partial pressures. The number of certain adsorbed species X at a certain T and P, $N_X(P,T)$, was calculated as below:

$$N_X(P,T) = \frac{e^{\left(\mu_X(P,T) - E_{ads,X}\right)/k_B T}}{\sum_X e^{\left(\mu_X(P,T) - E_{ads,X}\right)/k_B T}} \quad (2)$$

In equation 2, $\mu_X(P,T)$ is the chemical potential for pure-component gas-phase X at a given T and P, $E_{ads,X}$ denotes the binding energy (E_b) of adsorbed molecule X on the adsorbent, respectively. The chemical potentials of selected gases were obtained by interpolation of experimental values to the following expression:

$$\mu_X^{real}(P,T) = \mu_X^{ideal}(P,T) + (A_X + B_X \times T) \quad (3)$$

In equation 3, $\mu_X^{ideal}(P,T)$ indicate the chemical potential of an ideal, monoatomic gas X, A and B are fitted coefficient for the gas X (shown in Table 2), respectively. Thermochemical data of selected the gases were obtained from NIST standard reference database 23 [**47]** and two studies on ideal gas properties by Chao and co-workers **[48-50]**. Our cross-validation of these references showed less than a 0.5% error in comparison to the practical values. Two compositions of gas mixtures were suggested by considering saturated vapor pressure at atmospheric condition and referring a study on VOCs in the industrial facilities **[51]**. These conditions are presented in Table 3.

Figure 10 shows the occupancies of each gas in two types of mixture, for three types of adsorbent considered in this study, C_2N, GDY and C_2N···GDY heterostructure. In case of saturated vapor, Scenario 1 in Table 3, Figure 10 (a-c), the toluene and propanol have lower concentrations than ethanol and acetone, but their occupancies are dominant for three adsorbents due to their exponents in eq. 1, also known as Gibbs factor, are bigger than other gases, at given conditions. As shown in Figure 10(a-c), C_2N···GDY heterostructure has high selectivity for toluene in comparison with C_2N or GDY only; because of the E_b values are increased in C_2N···GDY heterostructure than the others. In more diluted gas, Scenario 2 in Table 3, Figure 10 (d-f), declines in occupancies are shifted to lower temperature than of saturated one owing to higher chemical potentials by lower partial pressures. It means, lower temperatures are needed so that the diluted VOCs molecules are captured on adsorbent. As shown in Figure 10(f) we see that the coverage of toluene on C_2N···GDY heterostructure is approximately 0.1% per unit cell. If this adsorbate

concentration and charge transfer are enough to detect the existence of VOCs, it could be used as a chemical sensor practically.

Inspection of table 1 shows that the strongest VOC physical binding is found in each case for acetone@C_2N, ethanol@C_2N, propanal@C_2N, and toluene@C_2N···GDY, respectively. For these cases we show the lack of ELF between the VOC and the 2D material (see Figure 11), as characterized by a deep-blue band separating them. This is conclusive evidence that none of the cases of VOC adsorption on C_2N, GDY or the C_2N···GDY heterostructure in this study are due to chemisorption, as no chemical bond ELF regions can detected for any of the interactions.

Conclusions

Density functional theory calculations with van der Waals correction were employed to study the structures, electronic and sensing properties of C_2N and GDY monolayers and further the C_2N···GDY heterostructure, with regard to binding to VOCs. On the basis of energetic analysis, we find that the selected VOCs, acetone, ethanol, propanal bind twice as strong on C_2N than on GDY monolayer. However, C_2N···GDY heterostructure in AB stacking with the interlay spacing of 3.54 Å binds all the selected VOCs with appropriate binding energies that fall within an ideal range of efficient sensing mechanism (-0.50 to -0.77 eV). Electron localization function analysis reveal that the binding of VOCs are in all cases due to physisorption and Bader charge analysis shows no (or negligible) charge transfer from the VOCs to the C_2N and GDY monolayers and C_2N···GDY heterostructure. The binding of the VOCs to the 2D material modifies the electronic characteristics of C_2N and GDY monolayers and C_2N···GDY heterostructure, which have been investigated by analysis of the density of states, and charge density difference. Finally, thermodynamic analysis of each of the VOCs on C_2N, GDY and C_2N···GDY heterostructure is carried out to determine the gas capacity and sensing mechanism under the practical conditions of pressure and temperature and also under varied compositions. These results suggest that the considered 2D systems, especially the C_2N···GDY heterostructure, are promising candidates for sensing materials for the selected VOCs under practical working conditions.

Acknowledgments

This research was undertaken with the assistance of resources from the National Computational Infrastructure (NCI), which is supported by the Australian Government. This work was supported by resources provided by the Pawsey Supercomputing Centre with funding from the Australian Government and the Government of Western Australia. AK acknowledges an Australian Research Council (ARC) Future Fellowship (FT170100373). HL acknowledges the National Institute of Supercomputing and Network/Korea Institute of Science and Technology Information with supercomputing resources including technical support (KSC-2018-C2-0028). RA would like to thanks the Carl Tryggers Stiftelse for Vetenskaplig Forskning (CTS) and Swedish Research Council (VR) for financial support. RA and DS acknowledge Olle Engkvists stiftelse, Sweden for financial support. JAL would like to thank the Swedish Research Council (VR), Knut and Alice Wallenberg Foundation, Kempe Foundations, Länsstyrelsen Norrbotten and Interreg Nord for financial support. SNIC and SNAC are acknowledged for providing the computing facilities.

References

1. T. Salthammer, Very volatile organic compounds: an understudied class of indoor air pollutants, *Indoor Air* 26, 25–38 (2016)

2. K. M. Tripathi, T. Y. Kim, D. Losic, T. T. Tung, Recent advances in engineered graphene and composites for detection of volatile organic compounds (VOCs) and non-invasive diseases diagnosis. *Carbon* **110**, 97-129 (2016)

3. J. Bartzis, P. Wolkoff, M. Stranger, G. Efthimiou, E.I. Tolis, F. Maes, A.W. Norgaard, G. Ventura, K.K. Kalimeri, E. Goelen, O. Fernandes, On organic emissions testing from indoor consumer products' use, *J. Hazard. Mater*. **285**, 37–45 (2015)

4. C. Zhang, Z-L. Hou, B-X. Zhang, H-M. Fang, S. Bi, High sensitivity self-recovery ethanol sensor based on polyporous graphene oxide/melamine composites, *Carbon* **137**, 467-474 (2018)

5. A. Mason, S.C. Mukhopadhyay, K.P. Jayasundera, Sensing technology: current status and future trends IV, *Smart Sens. Meas. Instrum*. **12**, 2194–

8402 (2015)

6. S. Sun, T. Hussain, W. Zhang, A. Karton, Blue phosphorene monolayers as potential nano sensors for volatile organic compounds under point defects. *Appl. Sur. Sci*. **486**, 52-57 (2019)

7. T. Hussain, B. Mortazavi, H. Bae, T. Rabczuk, H. Lee, A. Karton, Enhancement in hydrogen storage capacities of light metal functionalized Boron–Graphdiyne nanosheets. *Carbon* **147**, 199-205 (2019)

8. K. S. Novoselov, A. K. Geim, S. V. Morozov, D. Jiang, M. I. Katsnelson, I. V. Grigorieva, S. V. Dubonos and A. A. Firsov, Two-dimensional gas of massless Dirac fermions in graphene. *Nature* **438**, 197-200 (2005)

9. J. C. Meyer, A. K. Geim, M. I. Katsnelson, K. S. Novoselov, T. J. Booth and S. Roth, The structure of suspended graphene sheets. *Nature* **446**, 60-63 (2007)

10. S. Qi, X. Ma, B. Yang, L. Sun, W. Li, M. Zhao, Two-dimensional graphyne-like carbon nitrides: Moderate band gaps, high carrier mobility, high flexibility and type-II band alignment. *Carbon* **149**, 234-241 (2019)

11. X. Du, I. Skachko, A. Barker and E. Y. Andrei, Approaching ballistic transport in suspended graphene. *Nat. Nanotechnology* **3**, 491-495 (2008)

12. X. Fan, K. Elgammal, A. D. Smith, Mikael Östling, A. Delin, M. C. Lemme, F. Niklaus, Humidity and CO_2 gas sensing properties of double-layer graphene. *Carbon* **127**, 576-587 (2018)

13. M. G. Sanford, K. Yang, Y. Chyan, C. Kittrell, J. M. Tour, Laser-Induced Graphene for Flexible and Embeddable Gas Sensors. *ACS Nano* **13**, 3474-3482 (2019)

14. G. Cao, X. Liu, W. Liu, Q. Li, X. Li, X. Wang, Chemical environment dominated Fermi level pinning of a graphene gas sensor. *Carbon* **124**, 57-63 (2017)

15. F. A. L. de Souza, R. G. Amorim, J. Prasongkit, W. L. Scopel, R. H. Scheicher, A. R. Rocha, Topological line defects in graphene for applications in gas sensing. *Carbon* **129**, 803-808 (2018)

16. P. Panigrahi, A. K. Dhinakaran, Y. Sekar, R. Ahuja, T. Hussain, Efficient Adsorption Characteristics of Pristine and Silver-Doped Graphene Oxide

Towards Contaminants: A Potential Membrane Material for Water Purification. *ChemPhysChem* **19**, 2050-2057 (2018)

17. M. M. Haley, Synthesis and properties of annulenic subunits of graphyne and graphdiyne nanoarchitectures. *Pure Appl. Chem.* **80**, 519–532 (2008)

18. Z. Jia, Y. Li, Z. Zuo, H, Liu, C. Huang and Y. Li, Synthesis and Properties of 2D Carbon—Graphdiyne. *Acc. Chem. Res.* **50**, 2470–2478 (2017)

19. J. Mahmood, E. K. Lee, M. Jung, D. Shin, I-Y. Jeon, S-M. Jung, H-J. Choi, J-M. Seo, S-Y. Bae, S-D. Sohn, N. Park, J. H. Oh, H-J. Shin, N-B. Baek, Nitrogenated holey two-dimensional structures. *Nat. Comm*. **6**, 6486-6492 (2015)

20. Z. Meng, X. Zhang, Y. Zhang, H. Guo, Y. Wang, Q. Shi, D. Rao, Y. Liu, K. Deng and R. Lu, Graphdiyne as a High-Efficiency Membrane for Separating Oxygen from Harmful Gases: A First-Principles Study. *ACS Appl. Mater. Interfaces* **8**, 28166-28170 (2016)

21. M. Makaremi, B. Mortazavi, T. Rabczuk and C. V. Singh, Theoretical Investigation: 2D N-Graphdiyne Nanosheets as Promising Anode Materials for Li/Na Rechargeable Storage Devices. *ACS Appl. Nano Mater.***2**, 127-135 (2019)

22. P. Panigrahi, A. K. Dhinakaran, S. R. Naqvi, S. R. Gollu, R. Ahuja and T. Hussain, Light metal decorated graphdiyne nanosheets for reversible hydrogen storage. *Nanotechnology* **29**, 355401-355410 (2018)

23. Z-Z. Lin, Graphdiyne-supported single-atom Sc and Ti catalysts for high-efficient CO oxidation. *Carbon* **108**, 343-350 (2016)

24. Y. Zheng, Y. Chen, L. Lin, Y. Sun, H. Liu, Y. Li, Y. Du and N. Tang, Intrinsic magnetism of graphdiyne. *Appl. Phys. Lett*. **111,** 033101–5 (2017)

25. C. Huang, Y. Li, N. Wang, Y. Hue, Z. Zuo, H. Liu and Y. Li, Progress in Research into 2D Graphdiyne-Based Materials. *Chem. Rev*. **118**, 7744-7803 (2018)

26. Y. Jiao, A. J. Du, M. Hankel, Z. H. Zhu, V. Rudolph and S. C. Smith, Graphdiyne: A Versatile Nanomaterial for Electronics and Hydrogen Purification. *Chem. Commun*. **47**, 11843□11845 (2011)

27. Y. Jiao, A. J. Du, S. C. Smith, Z. H. Zhu and S. Z. Qiao, H_2 Purification by

Functionalized Graphdiyne- Role of Nitrogen Doping. *J. Matt. Chem. A* **3**, 6767-6771 (2015)

28. M. I. Hernandez, M. Bartolomei and J. Campos-Martinez, Transmission of Helium Isotopes through Graphdiyne Pores: Tunneling Versus Zero Point Energy Effects. *J. Phys. Chem. A* **119**, 10743□10749 (2015)

29. Z. S. Meng, X. R. Zhang, Y. D. Zhang, H. Q. Gao, Y. H. Wang, Q. Shi, D. W. Rao, Y. Z. Liu, K. M. Deng and R. F. Lu, Graphdiyne as a High-Efficiency Membrane for Separating Oxygen from Harmful Gases: A First-Principles Study. *ACS Appl. Mater. Interfaces*, **8**, 28166□28170 (2016)

30. C. Q. Zhu, H. Li, X. C. Zeng, E. G. Wang, S. Meng, Quantized Water Transport: Ideal Desalination through Graphyne-4 Membrane. *Sci. Rep*. 3, 3163 (2013)

31. D. W. Ma, Q. Wang, X. Yan, X. Zhang, C. He, D. Zhou, Y. Tang, Z. Lu and Z. Yang, 3 d transition metal embedded C_2N monolayers as promising single-atom catalysts: A first-principles study. *Carbon*, **105**, 463-473 (2016)

32. M. R. A. Kishore and P. Ravindran, Tailoring the Electronic Band Gap and Band Edge Positions in the C_2N Monolayer by P and As Substitution for Photocatalytic Water Splitting. *J. Phys. Chem. C* **121**, 22216-22224 (2017)

33. A. Befekry, C. Stampfl, M. Ghergherehchi, S. F. Shayesteh, A first-principles study of the effects of atom impurities, defects, strain, electric field and layer thickness on the electronic and magnetic properties of the C_2N nanosheet. *Carbon* **157**, 371-384 (2020)

34. G. Kresse and J. Hafner, Ab initio molecular dynamics for liquid metals. *Phys. Rev. B* **47**, 558-561 (1993)

35. G. Kresse and J. Hafner, Ab initio molecular-dynamics simulation of the liquid-metal–amorphous-semiconductor transition in germanium. *Phys. Rev. B* **49** 14251-14269 (1994)

36. G. Kresse and J. Hafner, Efficient iterative scheme for *ab initio* total-energy calculations using plane-wave basis set. *Phys. Rev. B* **54** 11169-11186 (1996)

37. J. P. Perdew, K. Burke and M. Ernzerhof, Generalized gradient approximation made simple. *Phys. Rev. Lett.* **77**, 3865-3868 (1996)

38. P. E. Blochl, Projector augmented-wave method. *Phys. Rev. B* **50**, 17953-17979 (1994)

39. S. Grimme, J. Antony, S. Ehrlich, H. Krieg, A consistent and accurate ab initio parametrization of density functional dispersion correction (DFT-D) for the 94 elements H-Pu, J. Chem. Phys. 2010, 132, 154104.

40. H. J. Monkhorst and J. D. Pack, Special points for Brillouin-zone integrations. *Phys. Rev. B* **13**, 5188-5192 (1976)

41. Y. Liu, Z. Meng, X. Guo, G. Xu, D. Rao, Y. Wang, K. Deng, R. Lu, Ca-Embedded C_2N: an efficient adsorbent for CO_2 capture. *Phys. Chem. Chem. Phys.*, **41**, 28323–28329 (2017)

42. S. J. Kim, H-J, Koh, C. E. Ren, O. Kwon, K. Maleski, S-Y, Cho, B. Anasori, C-K. Kim, Y-K. Choi, J. Kim, Y. Gogotsi, H-T. Jung, Metallic $Ti_3C_2T_x$ MXene Gas Sensors with Ultrahigh Signal-to-Noise Ratio. *ACS Nano* **12**, 986-993 (2018)

43. P. Ou, P. Song, X. Liu, J. Song, Superior Sensing Properties of Black Phosphorene as Gas Sensors: A Case Study on the Volatile Organic Compounds. *Adv. Theory and Simul. **2**,* 1800103-1800111 (2018)

44. V. Postica, A. Vahl, J. Strobel, D. S. Carballal, O. Lupan, A. C. Essadek, N. H. de Leeuw, F. Schutt, O. Polonsky, T. Strunskus, M. Baum, L. Kienle, R. Adelung, F. Faupel, Tuning doping and surface functionalization of columnar oxide films for volatile organic compound sensing: experiments and theory. *J. Mat. Chem. A* **6**, 23669-23682 (2018)

45. Y. Zhang, D. Li, L. Qin, D. Liu, Y. Liu, F. Liu, H. Song, Y. Wang, G. Lu, Preparation of Au-loaded TiO_2 pecan-kernel-like and its enhanced toluene sensing performance. *Sens. Actuators B: Chem*. **255**, 2240–2247 (2018)

46. M. R. A. Kishore, P. Ravindran, Enhanced Photocatalytic Water Splitting in a C_2N Monolayer by C-Site Isoelectronic Substitution. *ChemPhysChem* **18**, 1526-1532 (2017)

47. M. Long, L. Tang, D. Wang, Y. Li, Z. Shuai, Electronic structure and carrier mobility in graphdiyne sheet and nanoribbons: theoretical predictions. *ACS Nano* **5**, 2593-2600 (2011)

48. https://pages.nist.gov/REFPROP-docs/#referencing-the-refprop-program-in-publications

49. J. Chao, K. R. Hall, *Thermochim. Acta* **72,** 323-334 (1984)

50. J. Chao, K. R. Hall, K. N. Marsh and R. C. Wilhoit, *J. Phys. Chem. Ref. Data* **15**, 1369-1436 (1986)

51. T. Qin, X. Xu, T. Polak, V. Pacakova, K. Stulik and L. Jech, *Talanta* **44,** 1683-1690 (1997)

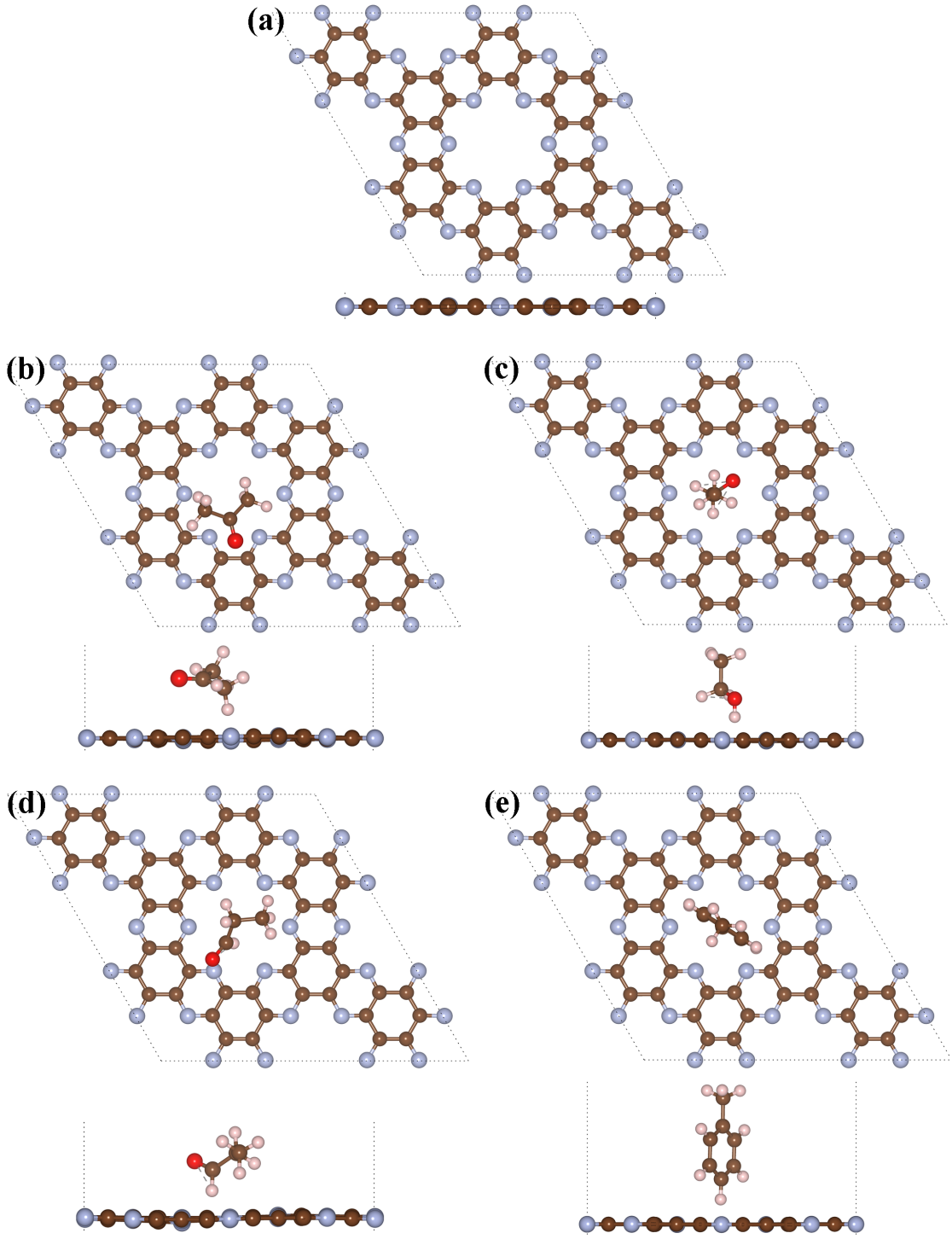

Figure 1. Optimized structures in top and side view of (a) pristine C_2N, and the strongest binding of (b) acetone@C_2N (c) ethanol@C_2N, (d) proponal@C_2N and (e) toluene@C_2N. Brown, silver, pink and red balls represent C, N, H and O atoms, respectively.

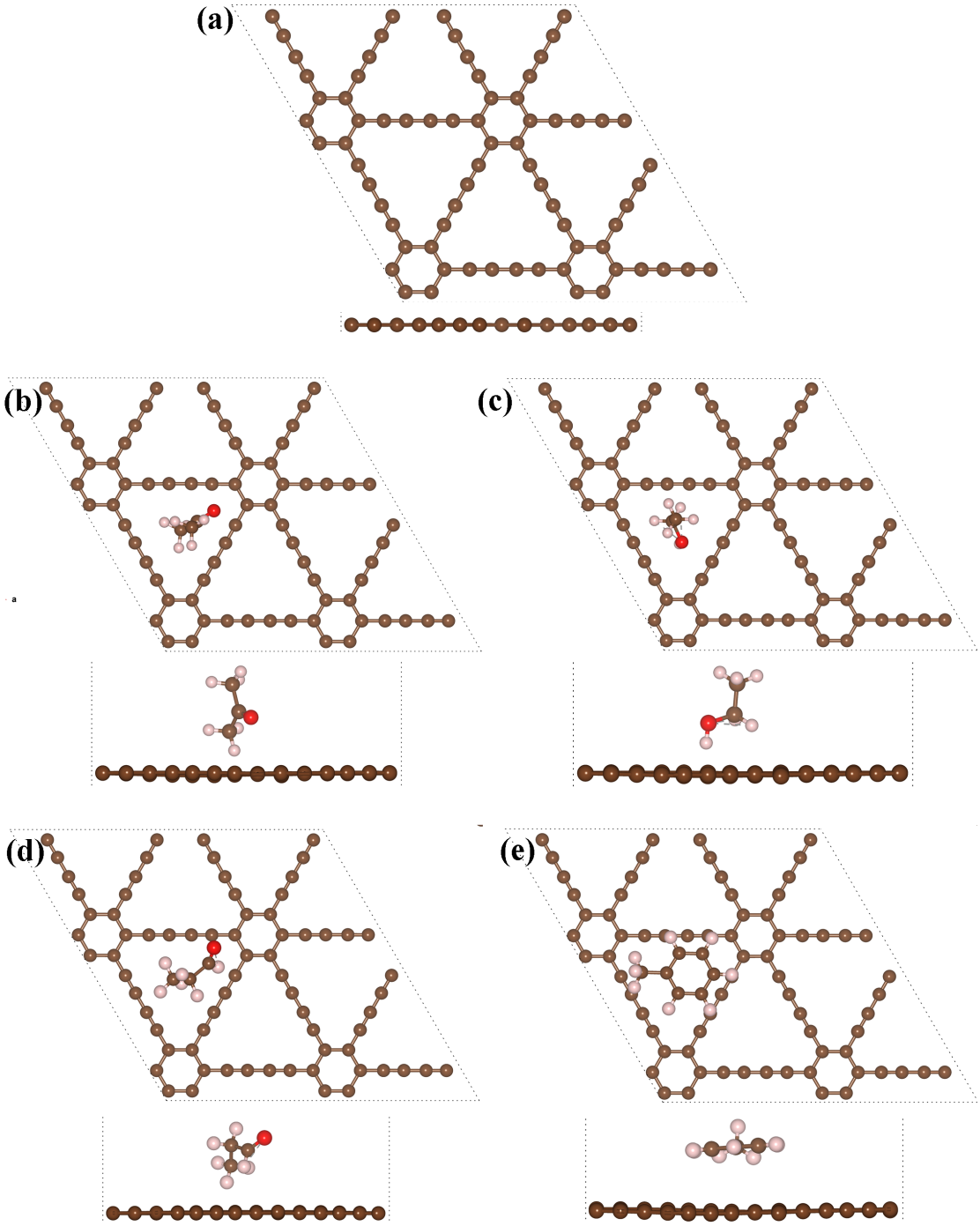

Figure 2. Optimized structures in top and side view of (a) Pristine GDY, and the strongest binding of (b) acetone@GDY (c) ethanol@GDY, (d) proponal@GDY and (e) toluene@GDY. Brown, pink and red balls represent C, H and O atoms, respectively.

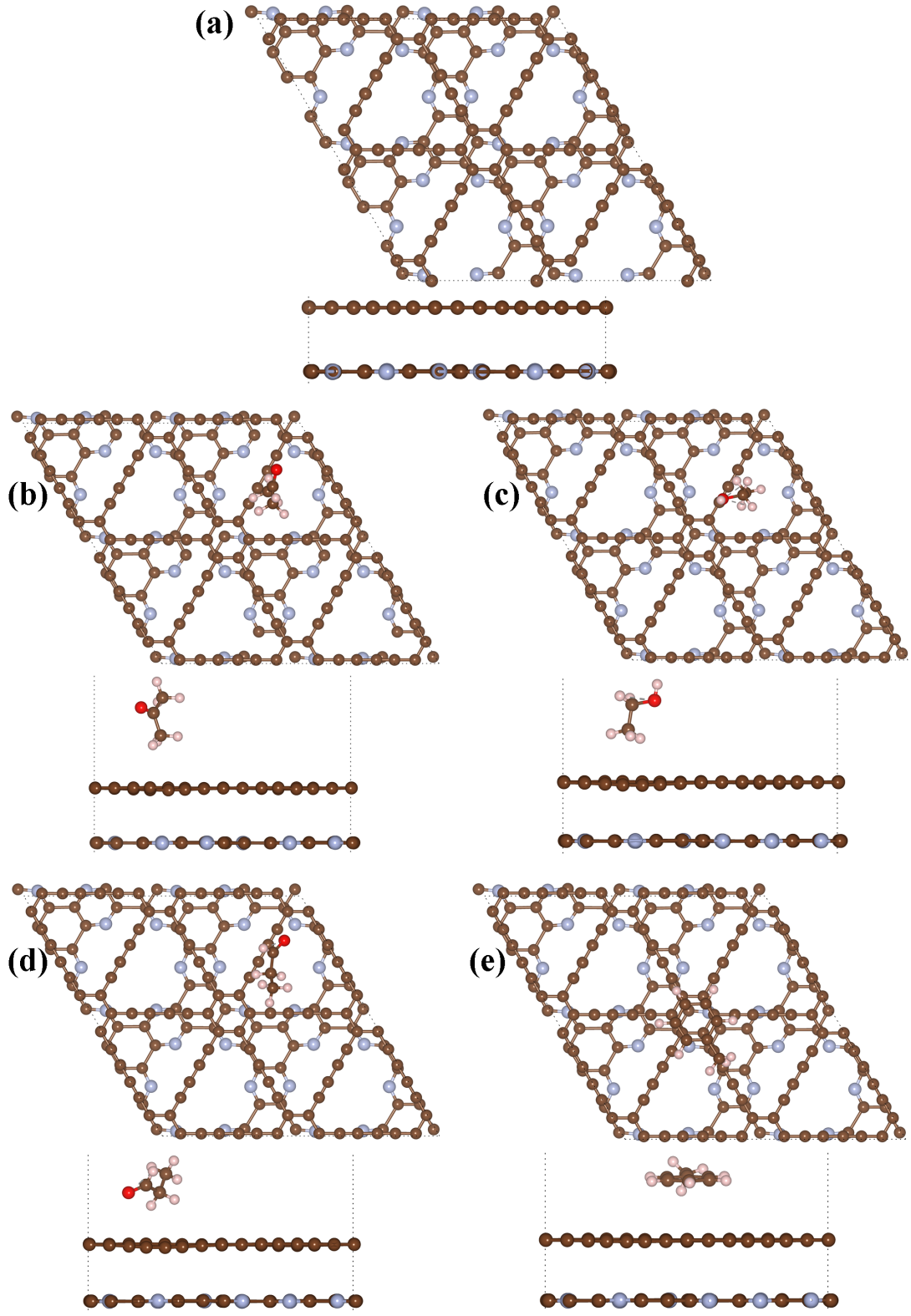
(a)
(b)
(c)
(d)
(e)

Figure 3. Optimized structures in top and side view of (a) pristine GDY···C_2N, and the strongest binding of (b) acetone@GDY···C_2N (c) ethanol@GDY···C_2N, (d) proponal@GDY···C_2N and (e) toluene@GDY···C_2N. Brown, silver, pink and red balls represent C, N, H and O atoms, respectively.

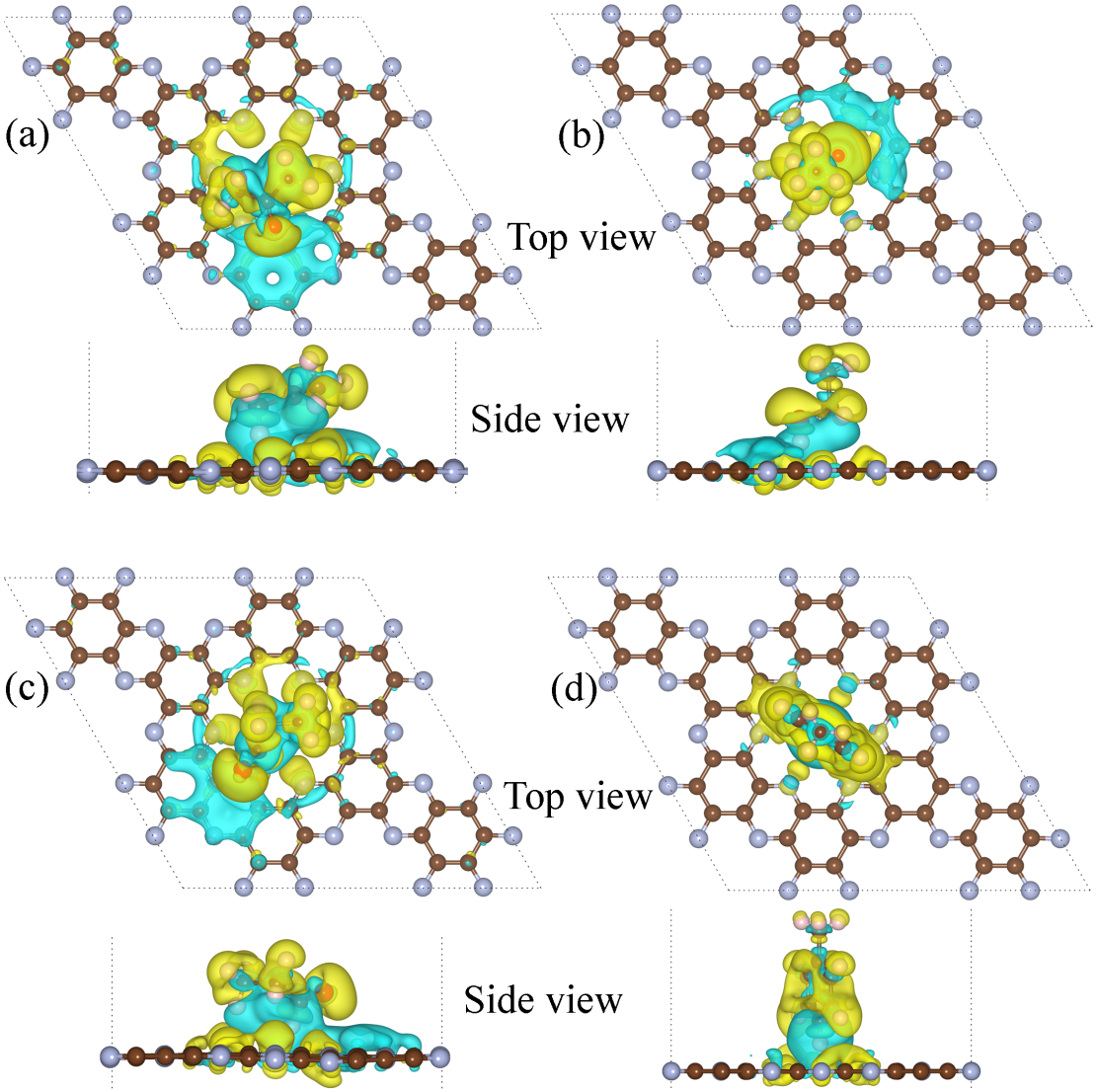

Figure 4. Isosurface charge density difference (CDD) in top and side view of (a) acetone@C_2N (b) ethanol@C_2N, (c) proponal@C_2N and (d) toluene@C_2N. Yellow and cyan colours represent accumulation and depletion of charges, respectively.

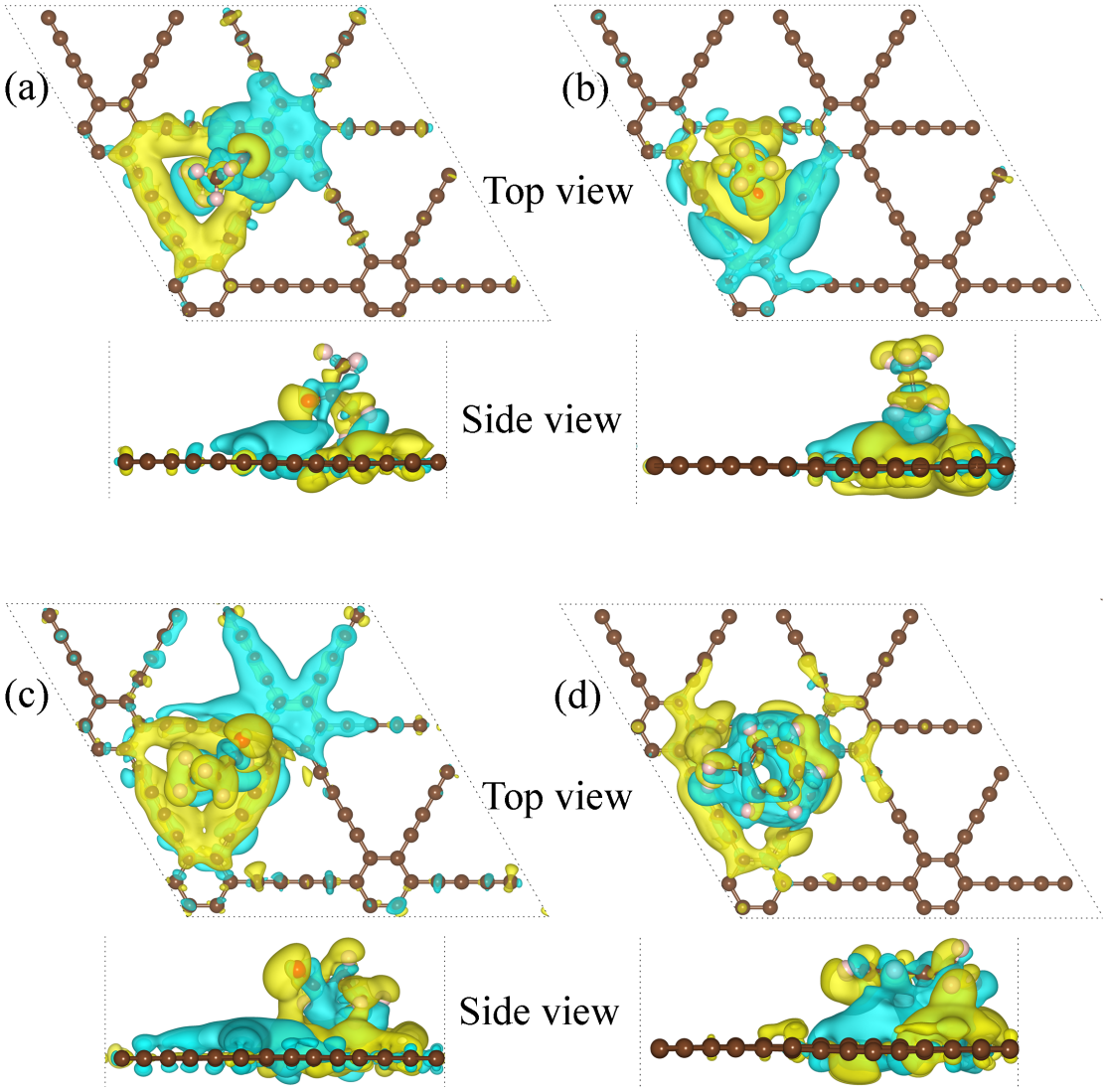

Figure 5. Isosurface charge density difference (CDD) in top and side view of (a) acetone@GDY (b) ethanol@GDY, (c) proponal@GDY and (d) toluene@GDY. Yellow and cyan colours represent accumulation and depletion of charges, respectively.

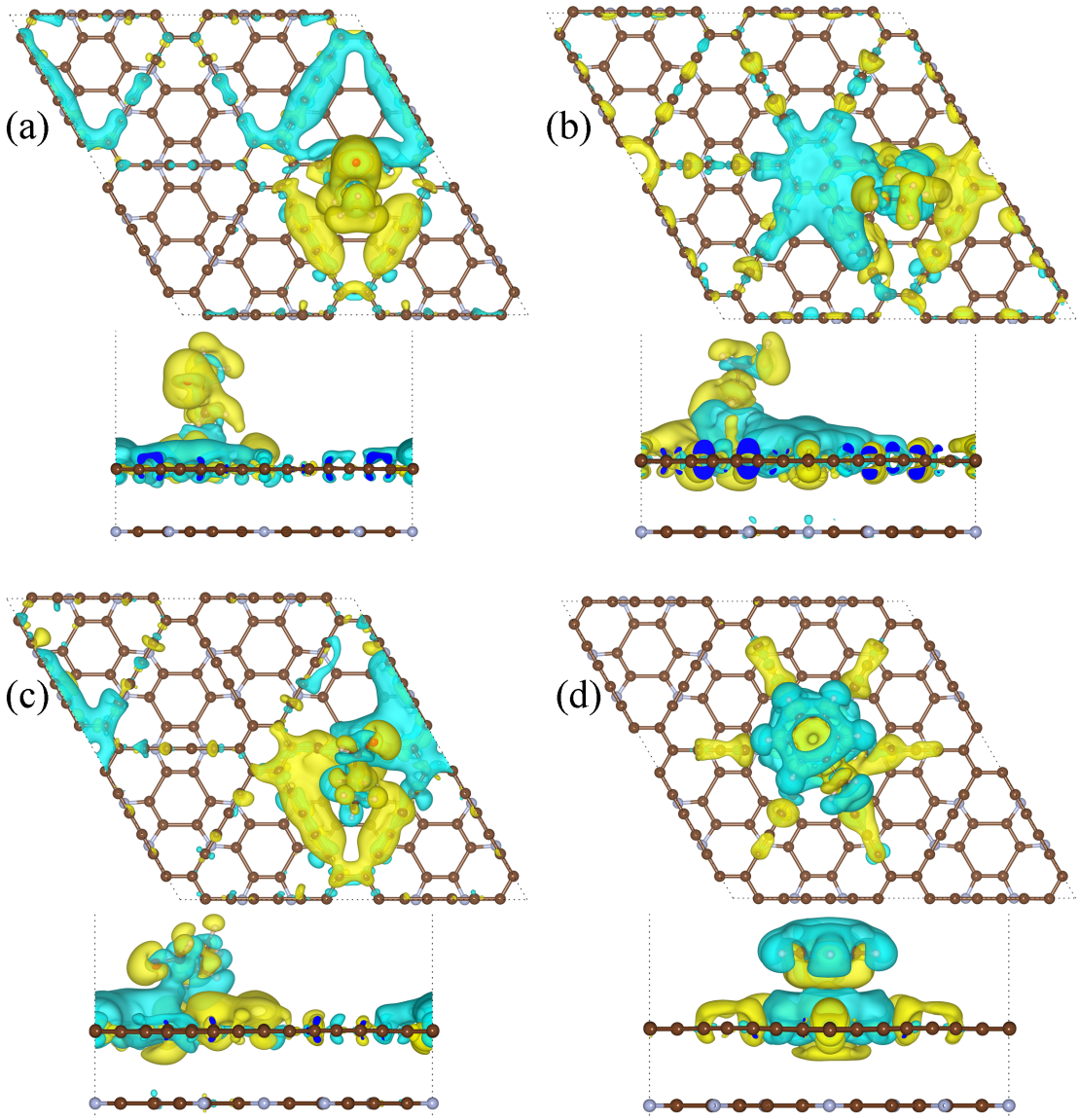

Figure 6. Isosurface charge density difference (CDD) in top and side view of (a) acetone@GDY···C_2N (b) ethanol@GDY···C_2N, (c) proponal@GDY···C_2N and (d) toluene@GDY···C_2N. Yellow and cyan colours represent accumulation and depletion of charges, respectively.

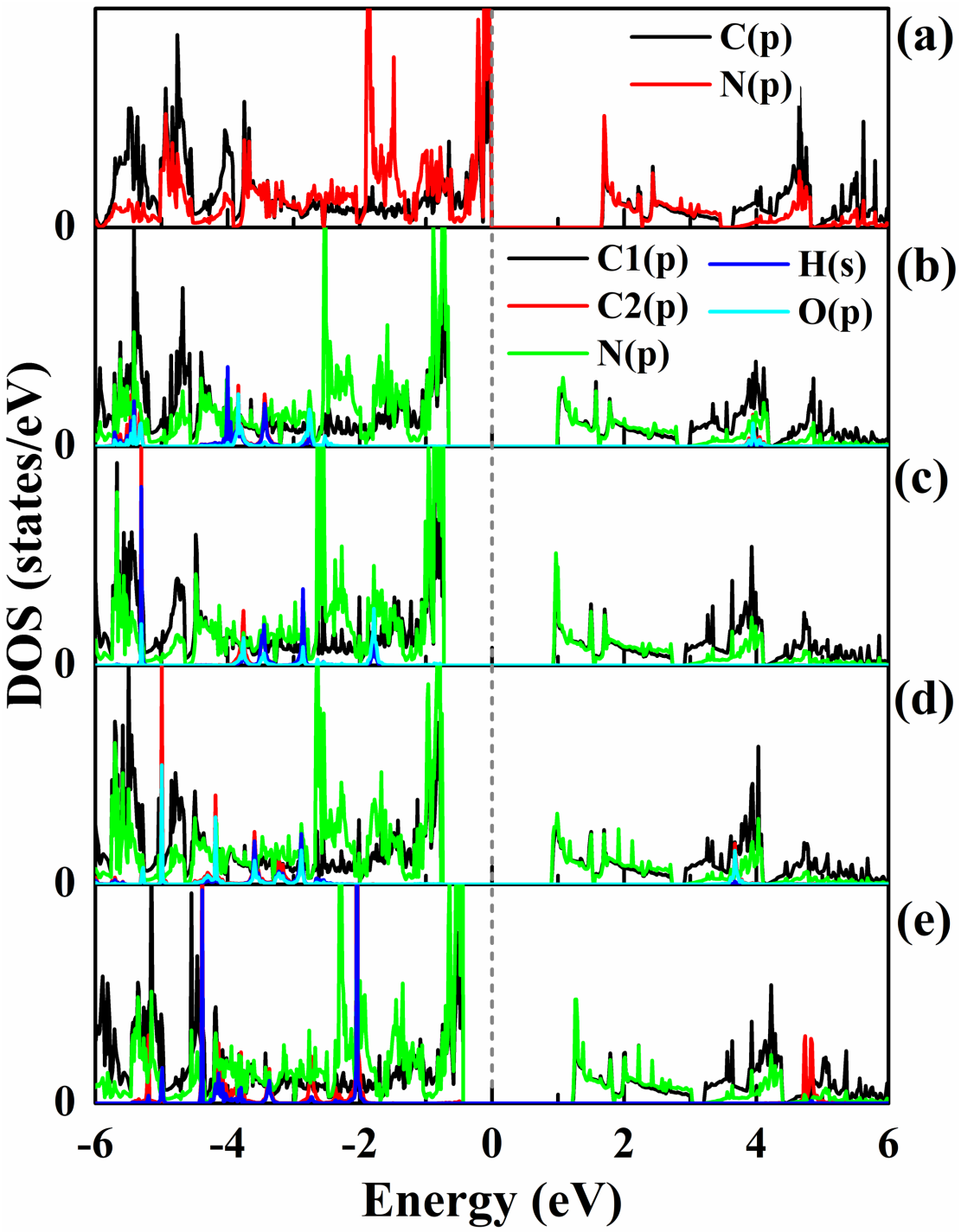

Figure 7. The projected density of states of (a) pristine C_2N monolayer and (b) acetone, (c) ethanol, (d) propanol and (e) toluene on the C_2N monolayer. Black, red, green, blue and cyan color represents the electronic orbitals of carbon atom of C_2N monolayer sheet, carbon atom of absorbed molecules, nitrogen, hydrogen and oxygen atom is also from absorbed molecules from Figure (b) to (e), respectively.

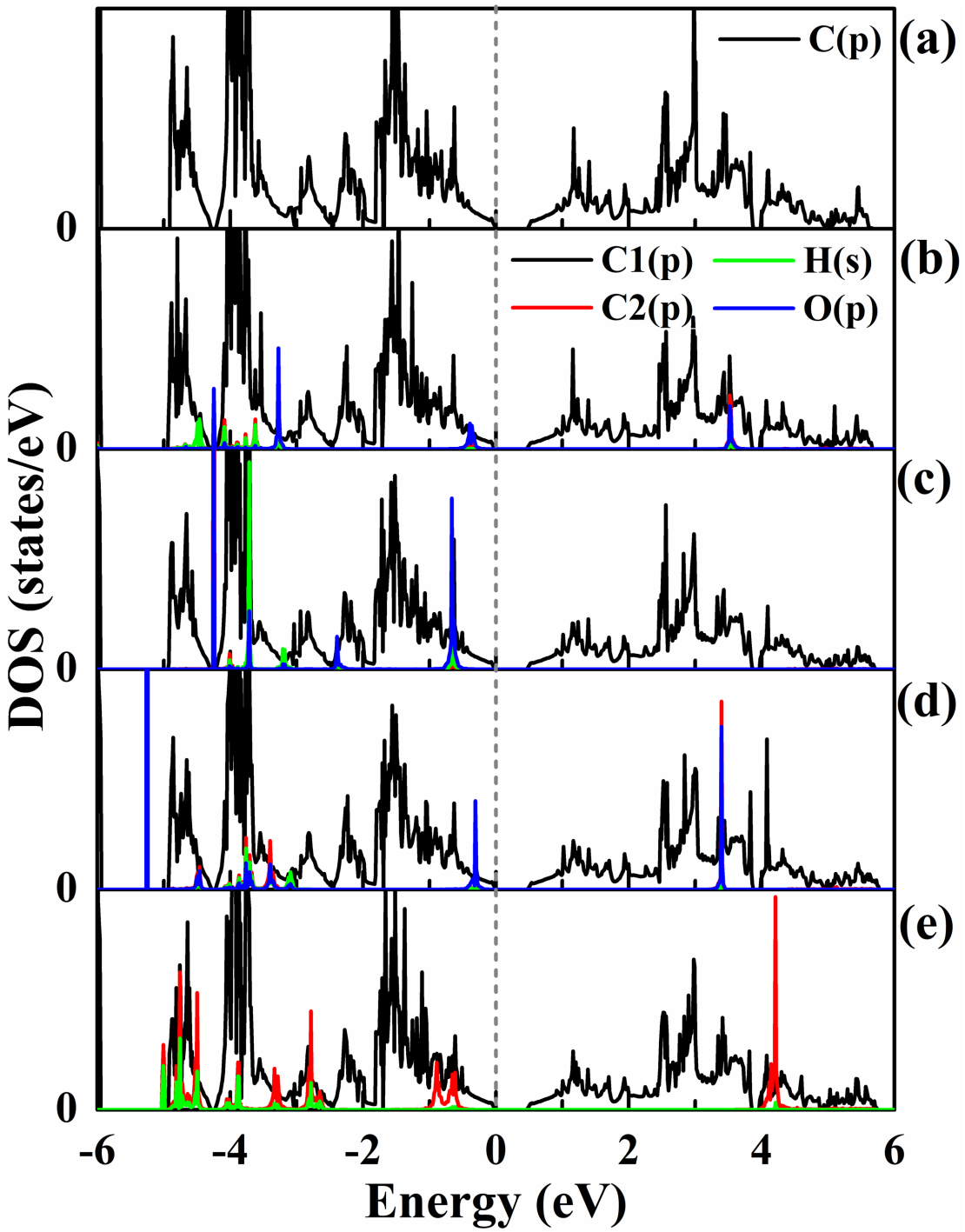

Figure 8. The projected density of states of (a) pristine GDY and (b) acetone, (c) ethanol, (d) propanol and (e) toluene on the surface of graphdiyne monolayer. Black, red, green and blue color represents the electronic orbitals of carbon atom of monolayer sheet, carbon atom of absorbed molecules, hydrogen and oxygen atom is also from absorbed molecules from Figure (b) to (e), respectively.

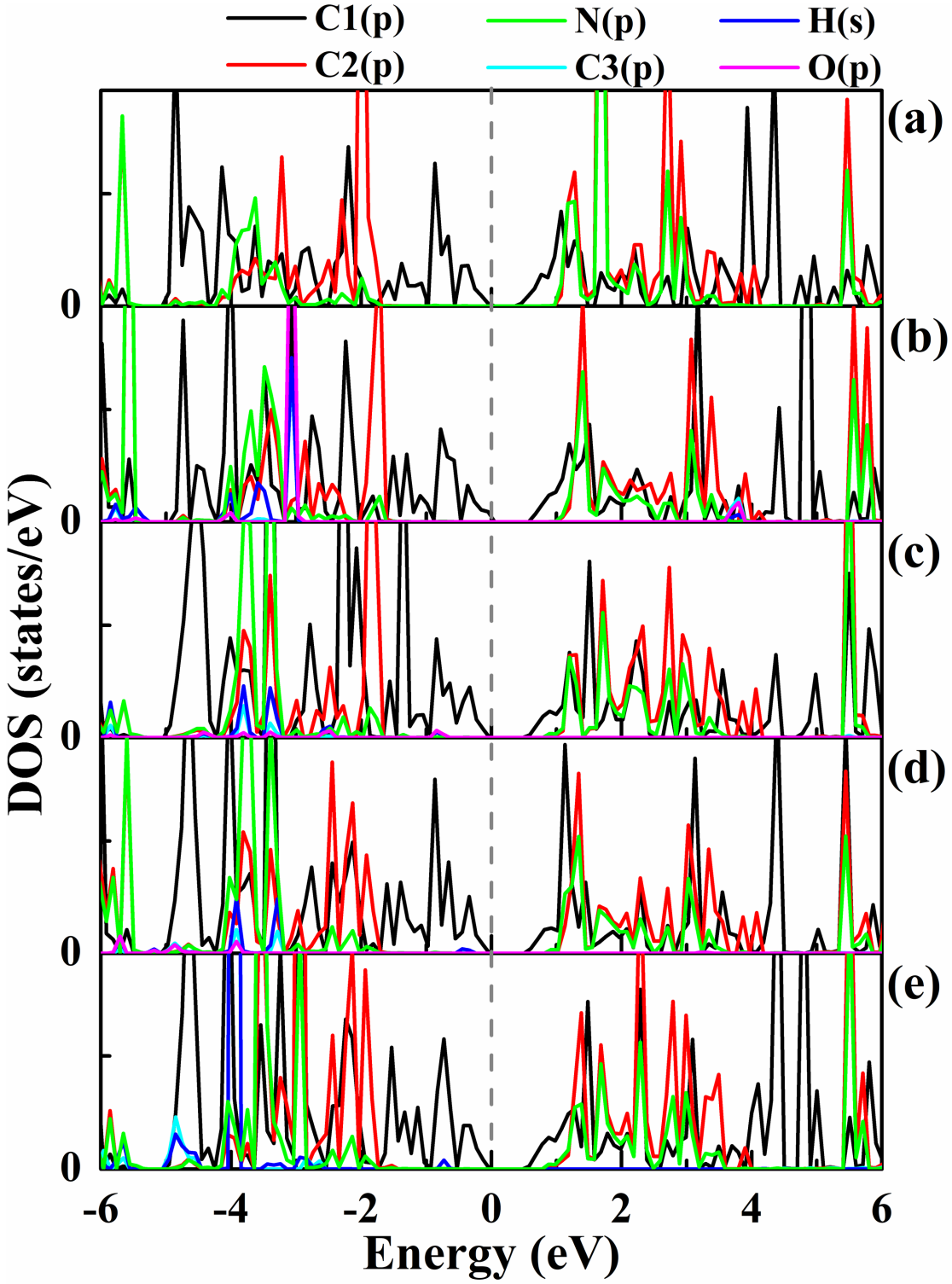

Figure 9. The projected density of states of (a) acetone, (b) ethanol, (c) propanol and (d) toluene on the surface of heterostructure of C_2N···GDY. The C1 (for GDY), C2 and N (for C_2N) symbol shows the density of states of Heterostructure represented by color black, red and green, respectively. The C3, H and O represent the density of states of interacting molecules with showing color cyan, blue and pink.

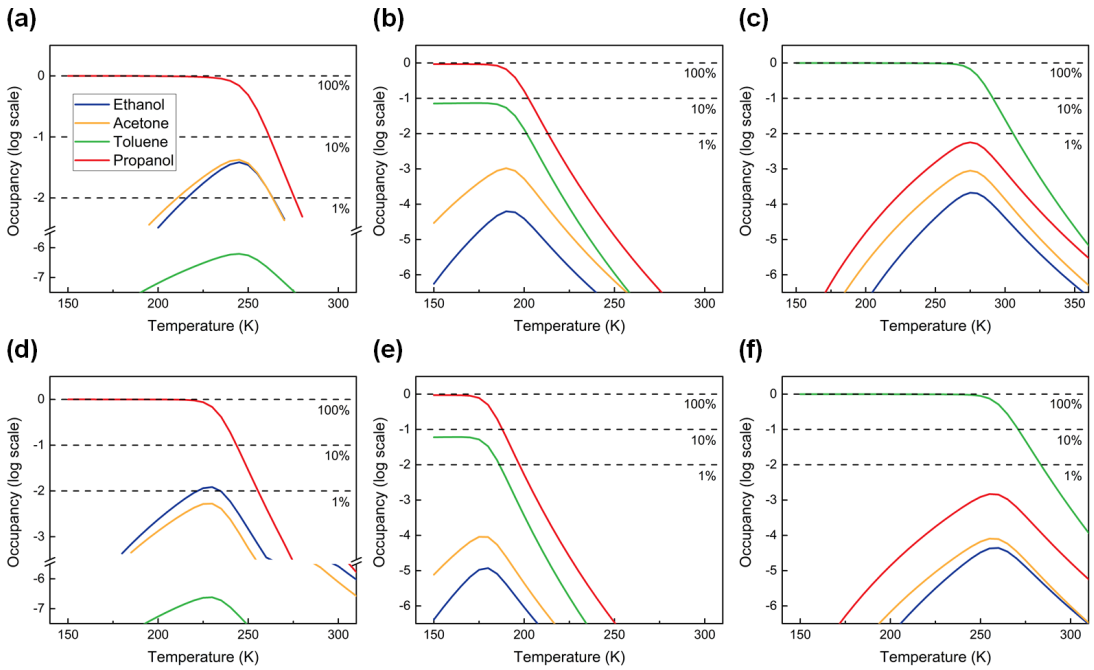

Figure 10. Adsorption-desorption process of VOCs mixtures on (a, d) C_2N monolayer, (b, e) GDY monolayer and (c, f) C_2N···GDY heterostructure layered structure. Gas compositions follow (a-c) the scenario 1 and (d-f) 2. Occupancy indicates the number of adsorbed gas molecule per adsorbent unit cell.

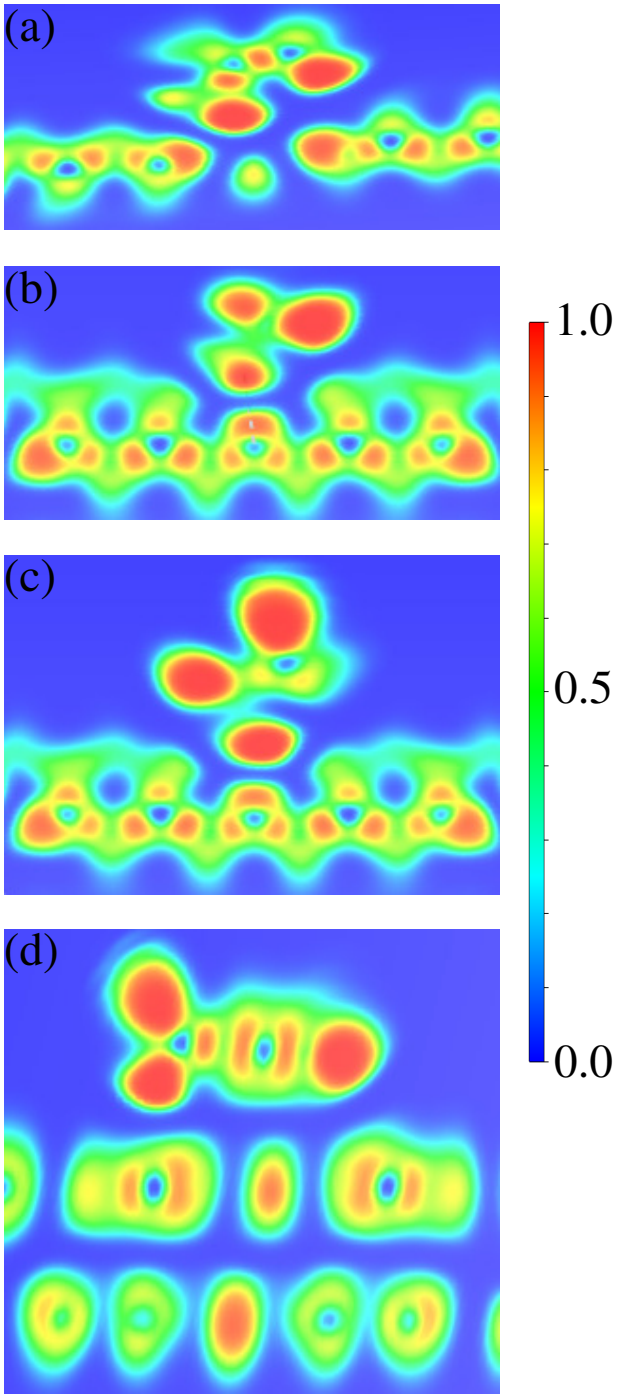

Figure 11. 2D electron localization function (ELF) cut through a plane including the shortest interaction for (a) acetone@C_2N, (b) ethanol@C_2N, (c) propanal@C_2N, and (d) toluene@C_2N···GDY heterostructure layered structure. ELF = 0 (blue) and 1 (red) values indicate vanishing and accumulation of electron density, respectively.

VOC	C_2N Monolayer		GDY Monolayer		C_2N···GDY Heterostructure	
	E_b (eV)	◘d (Å)	E_b (eV)	◘d (Å)	E_b (eV)	◘d (Å)
Acetone	-0.50	2.69	-0.25	2.88	-0.51	3.01
Ethanol	-0.52	2.53	-0.23	2.76	-0.49	3.02
Proponal	-0.52	2.42	-0.28	3.13	-0.57	2.96
Toluene	-0.40	2.99	-0.34	3.01	-0.77	2.86

Table 1. Binding energies (E_b) and the binding distances (Δd) of the selected VOCs on C_2N, GDY and C_2N···GDY heterostructure.

	A (eV)	*B* (meV)	R^2
Acetone	0.29637	-1.89742	0.99867
Ethanol	0.24489	-1.68118	0.99945
Propanol	0.50703	-2.39268	0.99917
Toluene	0.44229	-2.56035	0.99919

Table 2. The fitted coefficients of the chemical potentials of the real gases. These values are good to be fitted within 0.1 MPa to 0.1 kPa and 200 K to 700 K with a 0.5% error at the most.

	Scenario 1	Scenario 2
Acetone	0.302 atm.	2100 ppm
Ethanol	0.077 atm.	1500 ppm
Propanol	0.028 atm.	750 ppm
Toluene	0.038 atm.	850 ppm

Table 3. Scenario 1 is a combination of saturated vapor pressure at 298.15 K and 1 atm., and 2 were formed **[42]**.